EUROPEAN JOURNAL OF PURE AND APPLIED MATHEMATICS
2026, Vol. 19, Issue 2, Article Number 6623
ISSN 1307-5543 – ejpam.com
Published by New York Business Global

Thermal Transport in Combined Sutterby–Casson–Micropolar Flow via Exponential Curvature: A Regression-Based Numerical Study

Nadeem Abbas[1], Wasfi Shatanawi[1,*], M. Y. B. Mufarrej[1]

[1] *Department of Mathematics and Sciences, College of Humanities and Sciences, Prince Sultan University, Riyadh 11586, Saudi Arabia*

Abstract. We studied the flow of Sutterby–Casson micropolar fluid over an exponentially stretching curved sheet, including the effects of Soret and Dufour phenomena. A low Reynolds number magnetic field is considered to analyze its impact on the flow. The mathematical model is developed using boundary layer approximations, resulting in a system of partial differential equations (PDEs) based on relevant flow assumptions. These PDEs are then converted into ordinary differential equations (ODEs) via similarity transformations. The resulting ODEs are solved numerically. The results are presented with both graphs and tables, emphasizing how key physical parameters affect the flow behavior. Significant changes in the values of D_1 and C_1 indicate that the primary independent variable affecting heat and mass transfer shifts its behavior between $n = 0.0$ and $n = 0.5$. The large negative values of D_6 and C_6 suggest a dominant opposing factor within the system. When comparing $n = 0.0$ and $n = 0.5$, the system demonstrates a decreased sensitivity to changes in the independent variables. Additionally, the value of n influences heat and mass transfer mechanisms differently, which correspond to varying flow conditions and thermal properties.

2020 Mathematics Subject Classifications: 76D05, 76W05, 80A20, 65L10

Key Words and Phrases: Soret and dufour effects, sutterby–casson micropolar fluid, regression analysis, numerical analysis

1. Introduction

Sutterby [1] introduced a pioneering concept in fluid flow, offering a dynamic and adaptable framework that significantly enhances our understanding of fluid behavior. This innovative model holds substantial potential across various fields, including engineering and environmental sciences. As researchers continue to explore its complexities, the Sutterby fluid model is poised to transform our perception of non-Newtonian fluid dynamics and pave the way for future advancements in fluid flow analysis. The Sutterby liquid shows to be sort of non-Newtonian liquid, demonstrating that joins characteristics of both pseudoplastic and dilatant behaviors. A numerical demonstration typically illustrates and quantifies terms related to viscosity and shear rate. Such representation is valuable for understanding complex flow behaviors in various mechanical processes, including

*Corresponding Author.
DOI: https://doi.org/10.29020/nybg.ejpam.v19i2.6623

Email addresses: nabbas@psu.edu.sa (N. Abbas), wshatanawi@psu.edu.sa (W. Shatanawi), mfarrej@psu.edu.sa (M. Y. B. Mufarrej)

polymers and other non-Newtonian fluids. It is particularly important for predicting fluid responses under different shear stresses and flow conditions. Tetsu et al. [2] considered the natural convective phenomena for vertical isothermal surface using the Sutterby fluid model. The numerical outcomes have been presented of their analysis. Hayat et al. [3] developed the numerical results using the mixed model of Sutterby fluid and Peristaltic fluid flow. The convective boundary conditions are taken into account under the radiation and viscous dissipation. Sohail and Naz [4] considered the stretching cylinder and debated the results of Sutterby fluid using the Buongiorno model. They also find the results of MHD numerically. Ishtiaq et al. [5] debated the influence of Sutterby fluid flow using the variable magnetic field. They also considered the biaxially exponential/linear stretchable sheet and presented the results of slip phenomena. Recently, few models about non Newtonian fluid have been discussed for various assumptions (see Refs. [6, 7]).

The Soret and Dufour effects are two important phenomena in thermodynamics and transport processes. The Soret effect refers to the movement of different components in a mixture due to a temperature gradient. On the other hand, the Dufour impact includes the exchange of warm in a blend due to a concentration angle, which leads to vitality and mass exchange. This impact causes particles to move from a hot locale to a cold one or bad habit versa, depending on the nature of the blend.Alternately, the Dufour effect, also known as the diffusion-thermo effect, occurs when a temperature gradient arises from a concentration gradient in a mixture.Mass flow implies a temperature difference. The effects hold significance in various applications, such as diffusion in porous media, combustion processes, and chemical reactions. Proper consideration of Soret and Dufour effects ensures accurate modeling and analysis in these areas. Continuous research expands understanding of these phenomena and their implications in practical scenarios. The effects exert significant influence on fluid dynamics and heat transfer problems, extending beyond theoretical concepts into real-world impact, where they strongly alter heat and mass transfer rates. Proper consideration of these effects improves accuracy of simulations and predictions in systems involving heat and mass transport, rendering such knowledge highly valuable and essential for practical applications. Mortimer and Eyring [8] presented the initial theory of Soret and Dufour impacts. Theory of Soret and Dufour influence played an important role in the real life problem. Postelnicu [9] considered the natural convection using the Soret and Dufour impacts over a vertical permeable surface. The magnetic field has been implied to debate few effects under flow regions. These effects have highly effective and significant in the field of engineering and industrials. Partha et al. [10] considered the non-Darcy permeable surface to present the impacts of Soret and Dufour. Sardar et al. [11] examined the mixed convection flow of a Carreau nanofluid over a wedge and analyzed the impact of the Soret and Dufour effects. Jiang et al. [12] have studied the simultaneous heat and mass transfer processes, focusing on species interdiffusion and the coupled phenomena of the Soret and Dufour effects. Recent studies have explored various models of non-Newtonian fluids with influence of Soret and Dufour under different assumptions (see Refs. [[13]-[14]]).

It acts as a solid under low-stress conditions and as a fluid under high-stress environments. The Casson model, expressed as a function of yield stress and shear rate, defines the rheological properties of the fluid. Examples include ketchup and honey, widely applied in industries such as printing and food manufacturing. The Casson model enhances understanding and prediction of complex flow behavior across diverse applications. Mixed convective flow of a non-Newtonian Casson fluid over a vertical surface was deliberated by Vajravelu et al. [15]. Such analysis has investigated the behavior of fluids under several conditions. Mukhopadhyay et al. [16] examined the non-Newtonian characteristics of Casson fluids over an unsteady stretching surface. Oyelakin et al. [17] looked at Casson nanofluid flow over a stretching sheet, considering the effects of slip boundary conditions, convective heating, and thermal radiation. Kumar et al. [18] proposed a coupled stress model for time-dependent flow across a slippery curved surface, taking into account the magnetic dipole and non-Newtonian fluid. Furthermore, scholars have proposed an expanded version of Casson fluid theory for a variety of hypotheses (see Refs. [19, 20]).

The concept of a curved exponential stretching sheet presents intriguing features with numerous practical applications in science and engineering. A sheet extending exponentially along a curved surface enables precise control of material stretching and deformation. Such an arrangement significantly influences boundary layer flow, where dynamics involve varying pressure gradients and complex fluid behavior. An exponential stretching rate alters velocity distribution within the fluid, influencing flow stability and heat transfer characteristics. The property proves valuable for shaping and controlling objects and finds applications in fabric design, robotics, and biomedical research. Ability to generate complex shapes with controlled stretching establishes an essential tool for progress across multiple industries. Advancements with such technology promise wide-ranging developments in the future. Sajid and Hayat [21] studied the effects of thermal radiation on the laminar boundary layer flow over an exponentially extending sheet. Sahoo and Poncet [22] studied the 3rd grade fluid model under slip phenomena at exponential stretchable surfaces. Mustafa et al. [23] developed results on the analytical and numerical solution of nanofluid flow at exponential stretchable sheets. Okechi et al. [24] examined the flow behavior of a viscous fluid along an exponentially extending curved surface. Their research explored this complex scenario's fluid dynamics and heat transfer characteristics, providing insight into potential engineering applications involving curved geometries. Islam et al. [25] studied the entropy optimization of MHD nanofluid flow over a curved, exponentially stretching surface. The study focused on the effects of binary chemical reactions and Arrhenius activation energy. Ajaykumar et al. [26] investigated the entropy generation and optimized heat transfer features of Casson Williamson nanofluid flow over an exponentially stretching stratified curved sheet. Nadeem et al. [27] employed the finite element method to examine natural convection flow of Casson-based hybrid nanofluid (Al_2O_3–Cu/water) inside an H-shaped enclosure. Researchers have proposed an extended version of exponential stretching curved surfaces for different suppositions (Refs. [28, 29]).

In this study, we analyzed the behavior of a Sutterby micropolar Casson fluid flow over an exponentially stretching curved sheet. Our goal is to understand the complex interplay between Soret and Dufour effects within fluid dynamics. To achieve this, we pay particular attention to the influence of the magnetic field by using a significantly low magnetic Reynolds number. We also take into account the nuanced effects of heat generation to provide a comprehensive perspective on the fluid's behaviour. The results are presented in this analysis are unique and useful in the field of industrial and engineering. The following importance points are as:

- To explore the combined rheological features of Sutterby, micropolar, and Casson fluids in curved-sheet flow which offered the non-Newtonian fluid mechanics relevant to advanced material and biomedical processes.
- To investigate the Soret and Dufour effects which couple thermal and concentration gradients thereby enriching the understanding of heat and mass transfer in industrial and environmental applications.
- To assess the role of magnetic field influence and heat generation under practical low magnetic

Reynolds number conditions.

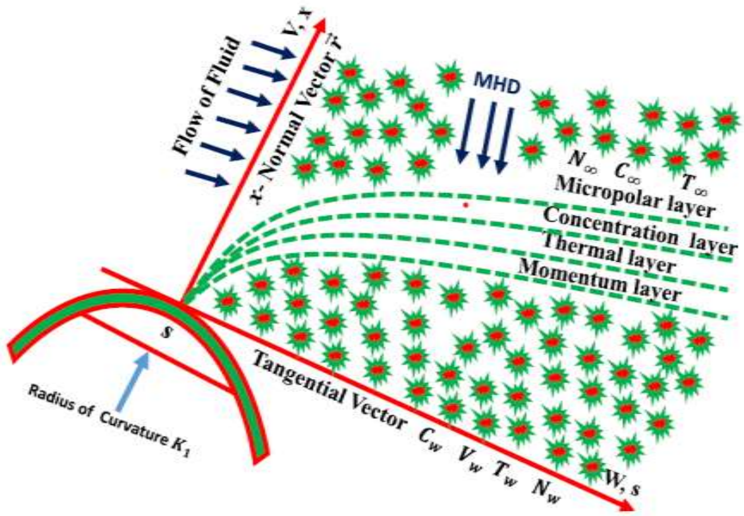

Figure 1: Flow diagram phenomena.

2. Mathematical formulation

We considered the couple stress in the extended version of SMC-fluid (Sutterby–Micropolar–Casson Fluid) model. The stretching is considered exponentially for curved surface. Figure 1 reports the geometry of flow phenomena. In this case, we considered few assumptions like as: the magnetic Reynolds number is not consider high because diminish the effects of electro-magnetic forces. The magnetic force is implemented vertically on the flow configurations. The components of radial and arc lengths are defined as x and S respectively. The curvature of curved sheet is defined as K_1. If the curvature tends to high, sheet become flat. V and W are components of radial and arc length directions. The vertex viscosity is k^*, magnetic force is B_0, Boltzmann contact is σ_0. The Soret and Dufour impacts have been consider in the present analysis. The boundary layer approximations were implemented to reduce the differential equations based on flow rules. The resulting partial differential equations are given below:

$$\frac{K_1}{x+K_1}(V)_x + \frac{1}{x+K_1}\big((x+K_1)W\big)_s = 0, \tag{2.1}$$

$$\frac{V^2}{x+K_1} = \frac{1}{\rho_f}P_x, \tag{2.2}$$

$$\begin{aligned} W(V)_x &+ \frac{K_1 V}{x+K_1}(V)_s + \frac{VW}{x+K_1} + \frac{1}{\rho_f}P_s \\ &= \frac{\nu_f}{2}\Big[(1+\tfrac{1}{\beta_0}+\Gamma_0)\big(V_{xx} - \frac{V}{(x+K_1)^2} + \frac{1}{x+K_1}V_x\big) - \frac{mN^2}{2}\big(V_x - \frac{V}{x+K_1}\big)^2 \\ &\big(V_{xx} + \frac{V}{3(x+K_1)^2} - \frac{1}{3(x+K_1)V_x}\big)\Big] - \frac{k^*}{(\rho)_f}N_x - \frac{\sigma_0 B_0^2}{(\rho)_f}V, \end{aligned} \tag{2.3}$$

$$W(N)_x + \frac{K_1 V}{x+K_1}(N)_s = \frac{\gamma^*}{(\rho j)_f}\big(N_{xx} + \frac{1}{x+K_1}N_x\big) - \frac{k^*}{(\rho j)_f}(2N + V_x + \frac{V}{x+K_1}), \tag{2.4}$$

$$W(T)_x + \frac{K_1 V}{x+K_1}(T)_s = \frac{1}{(\rho C_p)_f}\frac{k_f}{x+K_1}\big((x+K_1)T_x\big)_x + \frac{D_m K_t}{C_t(\rho C_p)_f}\frac{1}{x+K_1}\big((x+K_1)C_x\big)_x, \tag{2.5}$$

$$W(C)_x + \frac{K_1 V}{x+K_1}(C)_s = D_m\frac{1}{x+K_1}\big((x+K_1)C_x\big)_x + \frac{D_m K_t}{T_m}\frac{1}{x+K_1}\big((x+K_1)T_x\big)_x. \tag{2.6}$$

The boundary conditions are

$$\begin{aligned} &V = V_w, \quad W = 0, \quad T = T_w, \quad C = C_w, \quad N = -nV_x, \quad \text{at } x \to 0,\\ &V = 0, \quad V_x = 0, \quad T = T_\infty, \quad C = C_\infty, \quad N = 0, \quad \text{as } x \to \infty. \end{aligned} \tag{2.7}$$

To analyze boundary layer flow, a partial differential equation (PDE) is transformed into an ordinary differential equation (ODE). This involves scaling the system and reducing its dimensionality with similarity transformations. Using these transformations, I offer a general approach for rewriting the governing equations of boundary layer flow:

$$\begin{aligned} &T = T_\infty + e^{s/A}A\,(T_w - T_\infty)\,\theta(\xi), \qquad C = C_\infty + e^{s/A}A\,(C_w - C_\infty)\,\phi(\xi),\\ &\xi = x\sqrt{\frac{Be^{s/A}}{2\nu_f A}}, \qquad P = \rho_f B^2 e^{2s/A}\,p(\xi), \qquad N = Be^{3s/2A}\sqrt{\frac{B}{2A\nu_f}}\,g(\xi),\\ &V = Be^{s/A}f_\xi(\xi), \qquad W = -\frac{K_1}{x+K_1}e^{s/(2A)}\sqrt{\frac{B\nu_f}{2A}}\,\big(f(\xi) + \xi f_\xi(\xi)\big). \end{aligned} \tag{2.8}$$

The system was reduced following the transformations Eq. [8] applied to Eq. [1] to [7], we get:

$$p_\xi(\xi) = \frac{(f_\xi(\xi))^2}{\xi+\Gamma}, \tag{2.9}$$

$$\begin{aligned} &\frac{4\Gamma}{\xi+\Gamma}p(\xi) + p_\xi(\xi)\frac{\xi\Gamma}{\xi+\Gamma}\\ &\quad = \frac{1}{2}\Big(1 + \frac{1}{\beta_0} + \Gamma_0\Big)\left(f_{\xi\xi\xi}(\xi) + \frac{f_{\xi\xi}(\xi)}{\xi+\Gamma} - \frac{f_\xi(\xi)}{(\xi+\Gamma)^2}\right) - \frac{\xi+2\Gamma}{(\xi+\Gamma)^2}\Gamma f_\xi(\xi)f_\xi(\xi)\\ &\qquad + \frac{\Gamma}{\xi+\Gamma}f(\xi)f_{\xi\xi}(\xi) + \frac{\Gamma}{(\xi+\Gamma)^2}f(\xi)f_\xi(\xi) - \frac{\gamma}{4}\left(f_{\xi\xi}(\xi) - \frac{f_\xi(\xi)}{\xi+\Gamma}\right)^2\left[f^{(3)}(\xi) + \frac{f_\xi(\xi)}{3(\xi+\Gamma)^2} - \frac{f_{\xi\xi}(\xi)}{3(\xi+\Gamma)}\right]\\ &\qquad - Mf_\xi(\xi) - \Gamma_0 g_\xi(\xi), \end{aligned} \tag{2.10}$$

$$\left(1 + \frac{\Gamma_0}{2}\right)\left(\frac{g_\xi(\xi)}{\xi+\Gamma} + g_{\xi\xi}(\xi)\right) - \Gamma_0\left(2g(\xi) + \frac{f_\xi(\xi)}{\xi+\Gamma} + f_{\xi\xi}(\xi)\right) - \frac{3\Gamma}{\xi+\Gamma}g(\xi)f_\xi(\xi) + \frac{\Gamma}{\xi+\Gamma}f(\xi)g_\xi(\xi) = 0, \tag{2.11}$$

$$\frac{1}{\Pr}\Big(\frac{\theta_\xi(\xi)}{\xi+\Gamma} + \theta_{\xi\xi}(\xi)\Big) + \left(f(\xi)\frac{\Gamma}{\xi+\Gamma}\theta_\xi(\xi) - 2\theta(\xi)\frac{\Gamma}{\xi+\Gamma}f_\xi(\xi)\right) + Du\left(\frac{\phi\xi(\xi)}{\xi+\Gamma} + \phi_{\xi\xi}(\xi)\right) = 0, \tag{2.12}$$

$$\left(\frac{\phi_\xi(\xi)}{\xi+\Gamma}+\phi_{\xi\xi}(\xi)\right)+SrSc\Big(\frac{\theta_\xi(\xi)}{\xi+\Gamma}+\theta_{\xi\xi}(\xi)\Big)+Sc\left(f(\xi)\frac{\Gamma}{\xi+\Gamma}\phi_\xi(\xi)-2\phi(\xi)\frac{\Gamma}{\xi+\Gamma}f_\xi(\xi)\right)=0. \tag{2.13}$$

Related boundary conditions are

$$\begin{aligned}
&f(\xi)=0,\quad f_\xi(\xi)=1,\quad \theta(\xi)=1,\quad \phi(\xi)=1,\quad g(\xi)=-nf_{\xi\xi}(0),\quad \text{as } \xi\to 0,\\
&f_\xi(\xi)=0,\quad g(\xi)=0,\quad \theta(\xi)=0,\quad \phi(\xi)=0,\quad f_{\xi\xi}(\xi)=0,\quad \text{as } \xi\to\infty.
\end{aligned} \tag{2.14}$$

The equations mentioned above have been modified by removing the term ”pressure,” converting the system to a new form:

$$\begin{aligned}
&\frac{1}{2}\left(1+\frac{1}{\beta_0}+\Gamma_0\right)\left(f_{\xi\xi\xi\xi}(\xi)-\frac{f_{\xi\xi}(\xi)}{(\xi+\Gamma)^2}+\frac{f_\xi(\xi)}{(\xi+\Gamma)^3}+\frac{2f_{\xi\xi\xi}(\xi)}{\xi+\Gamma}\right)\\
&\quad-\frac{\gamma}{4}\Bigg[f_{\xi\xi\xi}(\xi)f_{\xi\xi}(\xi)+\frac{f_\xi(\xi)f_{\xi\xi}(\xi)}{(\xi+\Gamma)^2}-\frac{f_{\xi\xi}(\xi)f_{\xi\xi}(\xi)}{\xi+\Gamma}-\frac{f_\xi(\xi)f_\xi(\xi)}{(\xi+\Gamma)^3}\\
&\qquad-\frac{f_\xi(\xi)f_{\xi\xi\xi}(\xi)}{\xi+\Gamma}+\frac{f_{\xi\xi}(\xi)f_\xi(\xi)}{(\xi+\Gamma)^2}\Bigg]\left(f_{\xi\xi\xi}(\xi)+\frac{f_\xi(\xi)}{3(\xi+\Gamma)^2}-\frac{f_{\xi\xi}(\xi)}{3(\xi+\Gamma)}\right)\\
&\quad-\frac{\gamma}{4}\left(f_{\xi\xi}(\xi)-\frac{f_\xi(\xi)}{\xi+\Gamma}\right)^2\left(f_{\xi\xi\xi\xi}(\xi)+\frac{f_{\xi\xi}(\xi)}{3(\xi+\Gamma)^2}-\frac{2f_\xi(\xi)}{3(\xi+\Gamma)^3}-\frac{f_{\xi\xi\xi}(\xi)}{3(\xi+\Gamma)}+\frac{f_{\xi\xi}(\xi)}{3(\xi+\Gamma)^2}\right)\\
&\quad-\frac{1}{\xi+\Gamma}\frac{\gamma}{4}\left(f_{\xi\xi}(\xi)-\frac{f_\xi(\xi)}{\xi+\Gamma}\right)^2\left(f_{\xi\xi\xi}(\xi)+\frac{f_\xi(\xi)}{3(\xi+\Gamma)^2}-\frac{f_{\xi\xi}(\xi)}{3(\xi+\Gamma)}\right)\\
&\quad+\frac{\Gamma}{\xi+\Gamma}[f(\xi)f_{\xi\xi\xi}(\xi)]+\frac{\Gamma}{(\xi+\Gamma)^2}[f_{\xi\xi}(\xi)f(\xi)]-\frac{\Gamma}{(\xi+\Gamma)^3}[f(\xi)f_\xi(\xi)]\\
&\quad-\frac{3\Gamma}{\xi+\Gamma}[f_{\xi\xi}(\xi)f_\xi(\xi)]-\frac{3\Gamma}{(\xi+\Gamma)^2}[f_\xi(\xi)f_\xi(\xi)]-M\Big(\frac{f_\xi(\xi)}{\xi+\Gamma}+f_{\xi\xi}(\xi)\Big)\\
&\quad-\Gamma_0\Big(\frac{g_\xi(\xi)}{\xi+\Gamma}+g_{\xi\xi}(\xi)\Big)=0,
\end{aligned} \tag{15}$$

$$\Big(1+\frac{\Gamma_0}{2}\Big)\Big(\frac{g_\xi(\xi)}{\xi+\Gamma}+g_{\xi\xi}(\xi)\Big)-\Gamma_0\Big(2g(\xi)+\frac{f_\xi(\xi)}{\xi+\Gamma}+f_{\xi\xi}(\xi)\Big)-\frac{3\Gamma}{\xi+\Gamma}g(\xi)f_\xi(\xi)+\frac{\Gamma}{\xi+\Gamma}f(\xi)g_\xi(\xi)=0, \tag{16}$$

$$\frac{1}{Pr}\Big(\frac{\theta_\xi(\xi)}{\xi+\Gamma}+\theta_{\xi\xi}(\xi)\Big)+\Big(f(\xi)\frac{\Gamma}{\xi+\Gamma}\theta_\xi(\xi)-2\theta(\xi)\frac{\Gamma}{\xi+\Gamma}f_\xi(\xi)\Big)+Du\Big(\frac{\phi_\xi(\xi)}{\xi+\Gamma}+\phi_{\xi\xi}(\xi)\Big)=0. \tag{17}$$

$$\Big(\frac{\phi_\xi(\xi)}{\xi+\Gamma}+\phi_{\xi\xi}(\xi)\Big)+SrSc\Big(\frac{\theta_\xi(\xi)}{\xi+\Gamma}+\theta_{\xi\xi}(\xi)\Big)+Sc\Big(f(\xi)\frac{\Gamma}{\xi+\Gamma}\phi_\xi(\xi)-2\phi(\xi)\frac{\Gamma}{\xi+\Gamma}f_\xi(\xi)\Big)=0. \tag{18}$$

The relevant boundary conditions are

$$\begin{aligned} &f(\xi) = 0, \quad f_\xi(\xi) = 1, \quad \theta(\xi) = 1, \quad \phi(\xi) = 1, \quad g(\xi) = -n f_{\xi\xi}(\xi), \quad \text{as } \xi \to 0, \\ &f_\xi(\xi) = 0, \quad g(\xi) = 0, \quad \theta(\xi) = 0, \quad \phi(\xi) = 0, \quad f_{\xi\xi}(\xi) = 0, \quad \text{as } \xi \to \infty. \end{aligned} \tag{19}$$

When a fluid flows over a surface being stretched, three main physical quantities are important to consider: The skin friction coefficient represents the amount of drag experienced by the surface due to the fluid's viscosity. This coefficient is directly proportional to the surface's shear stress. The Nusselt number measures thermal transfer efficiency from the surface to the fluid, which is important for understanding the heat transfer rate. The Sherwood number indicates the effectiveness of mass diffusion by showing the mass transfer rate, such as the concentration of solutes, from the surface to the fluid. The following text introduces the physical quantities of the flow region:

$$C_f = \frac{\tau_{xs}}{\rho_f V_w^2}, \quad Nu = \frac{s q_w}{k_f (T_w - T_\infty)}, \quad Shu = \frac{s q_m}{k_f (C_w - C_\infty)}, \tag{20}$$

with

$$\begin{aligned} &\tau_{xs} = \frac{\mu_0}{2} \left\{ \left(1 + \frac{1}{\beta_0} + \Gamma_0\right) \left(V_x - \frac{V}{x + K_1}\right) + \Upsilon N - \frac{m N^2}{2} \left(V_x - \frac{V}{x + K_1}\right)^2 \right\}_{x=0}, \\ &q_m = -C_{x=0}, \quad q_w = -T_{x=0}. \end{aligned} \tag{21}$$

By Eq. [20] and Eq. [21], it turn into as:

$$\begin{aligned} C_f Re^{1/2} = \left(1 + \frac{1}{\beta_0} + \Gamma_0\right)\left(f_{\xi\xi}(0) + \frac{1}{\Gamma} + \Gamma_0\right) - \frac{\gamma}{4}\left(f_{\xi\xi}(0)^3 + 3\frac{f_{\xi\xi}(0)}{\Gamma^2} - 3\frac{f_{\xi\xi}(0)}{\Gamma} - \frac{1}{\Gamma^3}\right), \\ Nu\, Re^{-1/2} = -\theta_\xi(0), \qquad Shu\, Re^{-1/2} = -\phi_\xi(0). \end{aligned} \tag{22}$$

The Reynolds number is defined as

$$Re = \frac{V_w s}{\nu_f}.$$

3. Solution procedure

The bvp4c numerical technique is used to solve nonlinear higher-order differential equations that have specific boundary conditions. This method involves breaking down the intricate higher-order differential system into a system of first-order differential equations, which can then be solved numerically. The model's convergence is achieved by reducing the residual error and achieving the tolerance threshold. The steps involved in this numerical technique include the following:

$$\begin{aligned} &Y_1 = f(\xi); \quad Y_2 = f_\xi(\xi); \quad f_{\xi\xi}(\xi) = Y_3; \quad f_{\xi\xi\xi}(\xi) = Y_4; \quad f_{\xi\xi\xi\xi}(\xi) = YY1; \\ &Y_5 = g(\xi); \quad Y_6 = g_\xi(\xi); \quad g_{\xi\xi}(\xi) = YY2; \\ &\theta(\xi) = Y_7; \quad Y_8 = \theta_\xi(\xi); \quad \theta_{\xi\xi}(\xi) = YY3; \\ &\phi(\xi) = Y_9; \quad Y_{10} = \phi_\xi(\xi); \quad \phi_{\xi\xi}(\xi) = YY4; \end{aligned} \tag{23}$$

$$
\begin{aligned}
YY1 = &-\frac{1}{\frac{1}{2}\left(1+\frac{1}{\beta_0}+\Gamma_0\right)-\frac{\gamma}{4}\left[Y_3-\frac{Y_2}{\xi+\Gamma}\right]^2}\Bigg\{\frac{1}{2}\left(1+\frac{1}{\beta_0}+\Gamma_0\right)\left(-\frac{Y_3}{(\xi+\Gamma)^2}+\frac{Y_2}{(\xi+\Gamma)^3}\right.\\
&\left.+\frac{2Y_4}{\xi+\Gamma}\right)-\frac{\gamma}{4}\left[Y_3Y_4+\frac{Y_2Y_3}{(\xi+\Gamma)^2}-\frac{Y_3Y_3}{\xi+\Gamma}-\frac{Y_2Y_2}{(\xi+\Gamma)^3}-\frac{Y_2Y_4}{\xi+\Gamma}+\frac{Y_2Y_3}{(\xi+\Gamma)^2}\right][Y_4\\
&+\frac{Y_2}{3(\xi+\Gamma)^2}-\frac{Y_3}{3(\xi+\Gamma)}\Bigg]-\frac{\gamma}{4}\left[Y_3-\frac{Y_2}{\xi+\Gamma}\right]^2\left[\frac{Y_3}{3(\xi+\Gamma)^2}-\frac{2Y_2}{3(\xi+\Gamma)^3}-\frac{Y_4}{3(\xi+\Gamma)}+\frac{Y_3}{3(\xi+\Gamma)^2}\right]\\
&-\frac{1}{\xi+\Gamma}\frac{\gamma}{4}\left[Y_3-\frac{Y_2}{\xi+\Gamma}\right]^2\left[Y_4+\frac{Y_2}{3(\xi+\Gamma)^2}-\frac{Y_3}{3(\xi+\Gamma)}\right]+\frac{\Gamma}{\xi+\Gamma}[Y_1Y_4]+\frac{\Gamma}{(\xi+\Gamma)^2}[Y_3Y_1]\\
&-\frac{\Gamma}{(\xi+\Gamma)^3}[Y_1Y_2]-\frac{3\Gamma}{\xi+\Gamma}[Y_2Y_3]-\frac{3\Gamma}{(\xi+\Gamma)^2}[Y_2Y_2]-M\left(\frac{Y_2}{\xi+\Gamma}+Y_3\right)-\Gamma_0\left(\frac{Y_6}{\xi+\Gamma}+YY2\right)\Bigg\};
\end{aligned}
\tag{24}
$$

$$
YY2=\left(1+\frac{\gamma}{2}\right)^{-1}\left[-\gamma\left(2Y_5+\frac{Y_2}{\xi+\Gamma}+Y_3\right)-\frac{3\Gamma}{\xi+\Gamma}Y_5Y_2+\frac{\Gamma}{\xi+\Gamma}Y_1Y_6\right]-\frac{Y_6}{\xi+\Gamma}; \tag{25}
$$

$$
YY3=-Pr\left(Y_1\frac{\Gamma}{\xi+\Gamma}Y_8-2Y_7\frac{\Gamma}{\xi+\Gamma}Y_2\right)+Du\left(\frac{Y_{10}}{\xi+\Gamma}+YY4\right)-\frac{Y_8}{\xi+\Gamma}; \tag{26}
$$

$$
YY4=-\left(SrSc\left(\frac{Y_8}{\xi+\Gamma}+YY3\right)+Sc\left(Y_1\frac{\Gamma}{\xi+\Gamma}Y_{10}-2Y_9\frac{\Gamma}{\xi+\Gamma}Y_2\right)\right)-\frac{Y_{10}}{\xi+\Gamma}; \tag{27}
$$

The boundary condition at surface:

$$
\begin{aligned}
&Y0(1);\quad Y0(2)-1;\quad Y\infty(3);\quad Y\infty(2);\quad Y0(5)+nY0(3);\quad Y\infty(5);\\
&Y0(7)-1;\quad Y\infty(7);\quad Y0(9)-1;\quad Y\infty(9).
\end{aligned}
\tag{28}
$$

3.1. Regression analysis

The optimization technique takes into account physical factor as essential elements. The quadratic equation consists of linear, square, and interaction terms involving key elements, as follows:

$$
\begin{aligned}
ShuRe^{-1/2} &= C_1+C_2Sr+C_3Du+C_4Sr^2+C_5Du^2+C_6SrDu,\\
NuRe^{-1/2} &= D_1+D_2Sr+D_3Du+D_4Sr^2+D_5Du^2+D_6SrDu.
\end{aligned}
\tag{29}
$$

Where, $D_1, D_3, D_2, D_4, D_6, D_5$ are regression coefficients line for Nusselt number. $C_1, C_2, C_3, C_4, C_6, C_5$ are regression coefficients line for Sherwood number. Thus, the model assists in evaluating the various components that interact and influence the response variables, specifically the Nusselt number and Sherwood number. Equation (29) shows that the variables Du and Sr influence both convective heat transfer and skin friction. The estimated coefficients are defined in Table 1.

Table 1: Estimated coefficients (RC) of the Regression line for Sherwood and Nusselt number.

Regression coefficient	D_1	D_2	D_3	D_4	D_5	D_6
$NuRe^{-1/2}$ (n=0.0)	-1.0476	18.6611	18.6648	0.163634	0.0338	-91.5574
$NuRe^{-1/2}$ (n=0.5)	1.0805	7.9743	7.978	0.0522	0.0338	-38.1227
Regression coefficient	C_1	C_2	C_3	C_4	C_5	C_6
$ShuRe^{-1/2}$ (n=0.0)	-0.3357	5.8365	6.8013	-0.1656	-0.003	-34.166
$ShuRe^{-1/2}$ (n=0.0)	0.5854	1.1904	2.1545	-0.1658	-0.003	-10.9323

Significant changes in the values of D_1 and C_1 indicate that the primary independent variable affecting heat and mass transfer shifts its behavior between $n = 0.0$ and $n = 0.5$. The large negative values of D_6 and C_6 suggest a dominant opposing factor within the system. When comparing $n = 0.0$ and $n = 0.5$, the system demonstrates a decreased sensitivity to changes in the independent variables. Additionally, the value of n influences heat and mass transfer mechanisms differently, which correspond to varying flow conditions and thermal properties.

4. Results and discussion

The numerical scheme presented in detail above has solved the nonlinear coupled differential equations system. The major outcomes have been presented through graphs and tabular form. The variation of involving physical factors on the temperature, velocity and concentration are presented in Figs. 2-9. Figure 2 presents the relationship between the Casson fluid factor and velocity. Velocity curves show lesser values for the casson fluid factor. Casson fluid revealed shear thinning behavior, which decreased viscosity with increasing shear rate. As the Casson fluid parameter increased and the impact on flow dynamics became more pronounced which led to a greater velocity decline. Figure 3 illustrates the correlation between the sutterby fluid factor and velocity. Velocity curves show higher values for the sutterby fluid factor. Sutterby fluid parameter increased, which led to an increase in the velocity of the fluid close to the stretching surface. These changes occurred because the fluid resistance to deformation decreased, allowing it to flow more freely. As a result, the velocity within the boundary layer can increase. Figure 4 illustrates the correlation between the magnetic field and velocity. Velocity declined with increasing magnetic field values. The Lorentz force acted perpendicular to the fluid velocity and the magnetic field direction. These forces opposed the fluid motion and provided a resistive effect on the fluid flow. As the magnetic field strength increased and the Lorentz force magnitude also increased. The result is greater resistance to flow. Figure 5 illustrates the correlation between the micropolar fluid factor and velocity. Velocity become low due to enrich values of 12 micropolar factor. As the rotation of fluid increased which declined the fluid velocity at surface. Figure 6 discusses the impact of both temperature and the Dufour effect. Temperature are noted to be declining for higher values of Dufour effect. As a result of transfer, the high-concentration regions have had higher temperatures and lost heat energy. This loss of energy caused into decrease in temperature in these regions. Figure 7 discusses the impact of both temperature and the Prandtl number. Temperature are noted to be declining for higher values of Prandtl number. As the Prandtl number increased, the fluid conducted less heat relative to its motion. A higher Prandtl number also formed a thicker thermal boundary layer. As a result, the heat transfer rate decreased. Figure 8 discusses the impact of both temperature and the soret effect. Temperature are noted to be enriching for higher values of soret effect. The Soret effect occurred when a temperature gradient drove mass diffusion in a fluid. A stronger Soret effect and a higher temperature gradient produce greater mass transport. This concentration change raised the fluid temperature in regions. In such areas, heat transfer is enhanced. Figure 9 discusses the impact of both concentration and the soret effect. Concentration are noted to be enriching for higher values of soret effect. The Soret effect generated a stronger thermophoretic force when the temperature gradient increased. This force enhanced mass diffusion in the fluid. As a result, solute accumulated more in regions with high temperature gradient. Over all, the strong concentration $n = 0.0$ achieved higher velocity and low temperature as compared to low concentration $n = 0.5$. Figs. 10-11 reported the variation of Nusselt and Sherwood number for different values of soret and Dufour effects.

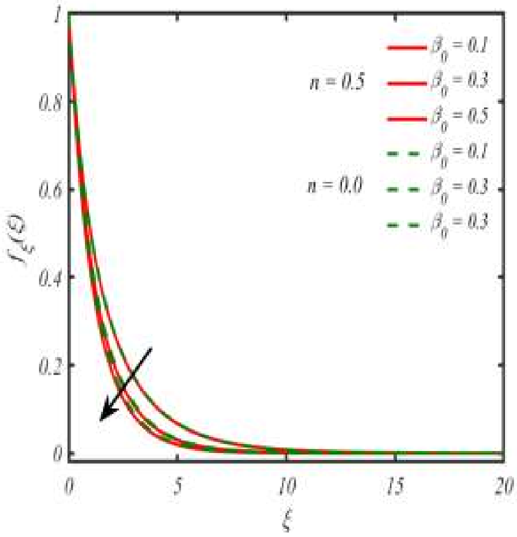

Figure 2: Variation of β_0 with $f_\xi(\xi)$.

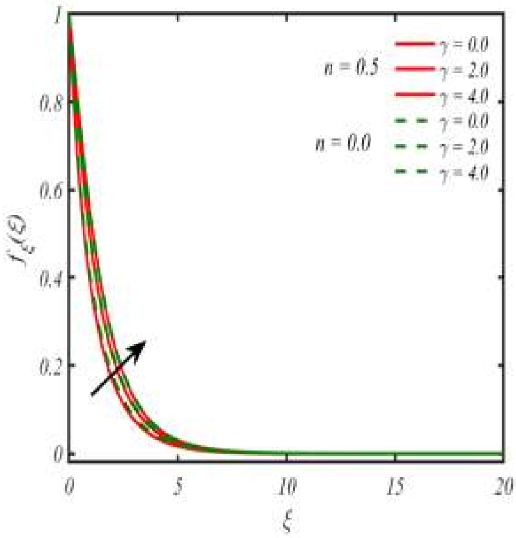

Figure 3: Variation of γ with $f_\xi(\xi)$.

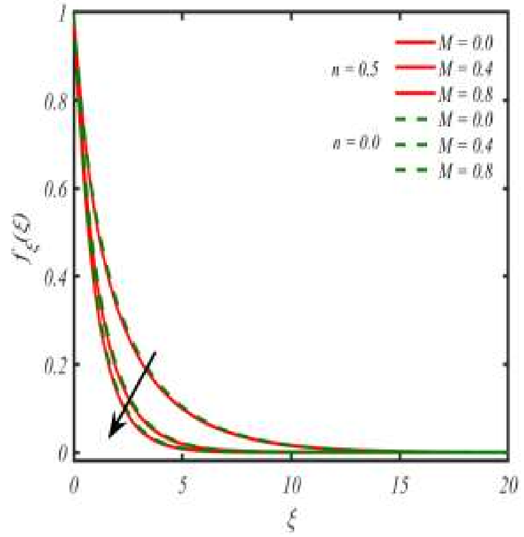

Figure 4: Variation of M with $f_\xi(\xi)$.

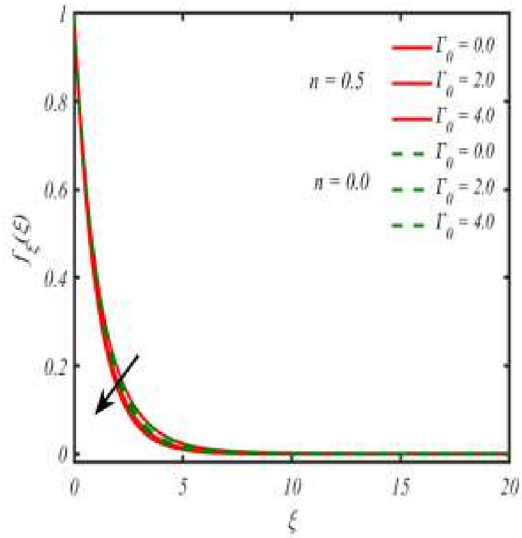

Figure 5: Variation of Γ_0 with $f_\xi(\xi)$.

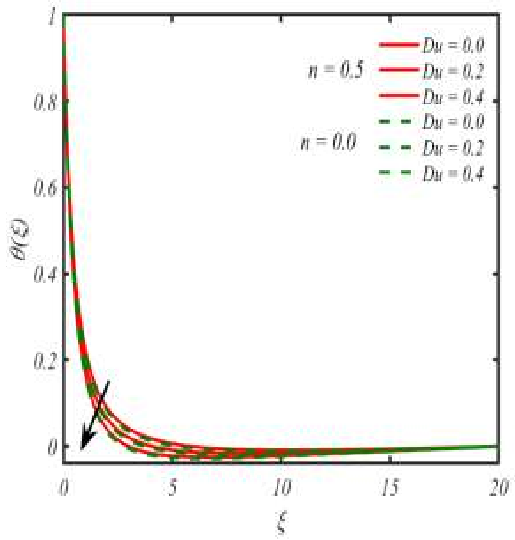

Figure 6: Variation of Du with $\theta(\xi)$.

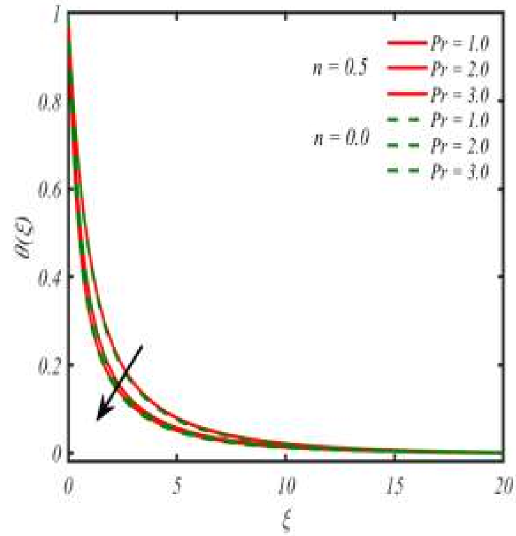

Figure 7: Variation of Pr with $\theta(\xi)$.

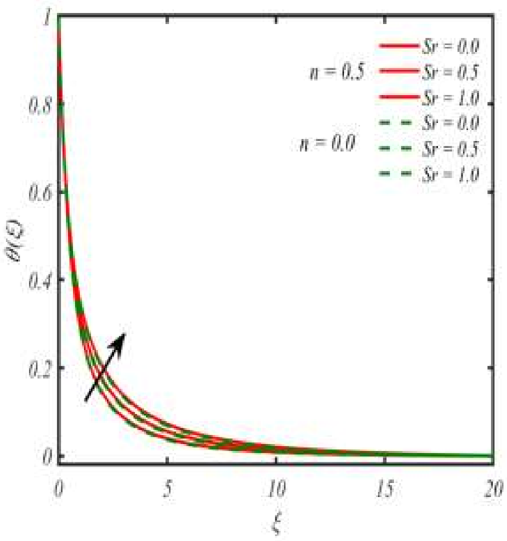

Figure 8: Variation of Sr with $\theta(\xi)$.

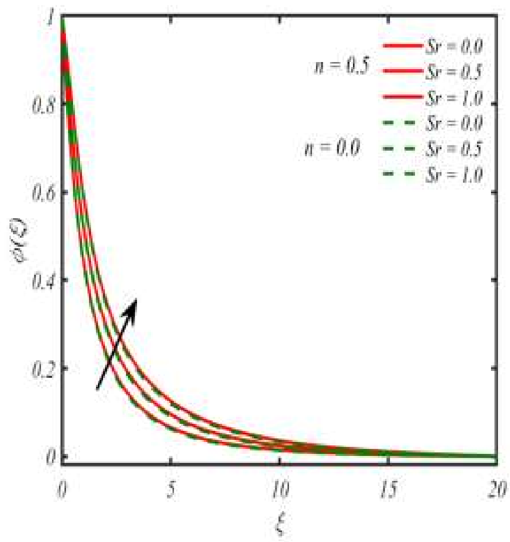

Figure 9: Variation of Sr with $\phi(\xi)$.

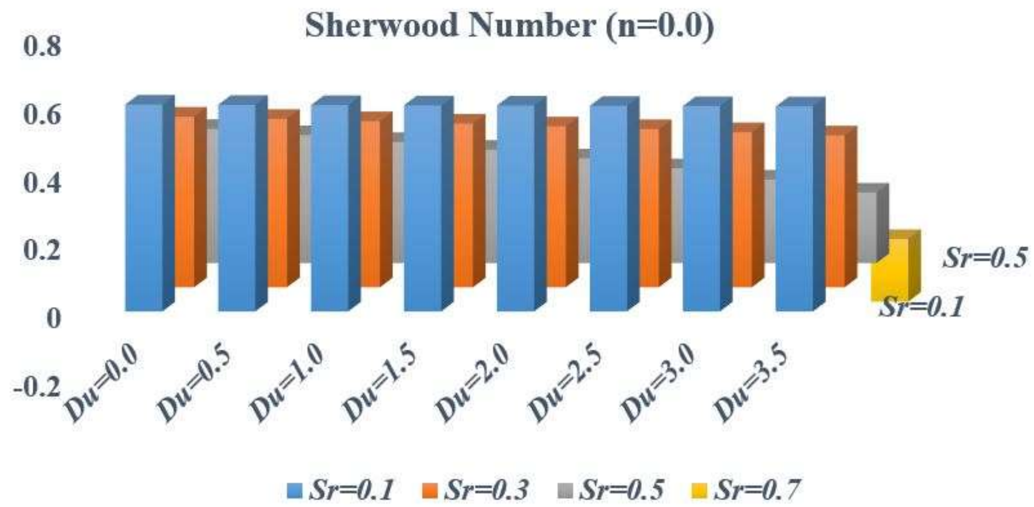

Figure 10: Variation of Sherwood number for different values of Dufour and Soret effects for $n = 0.0$.

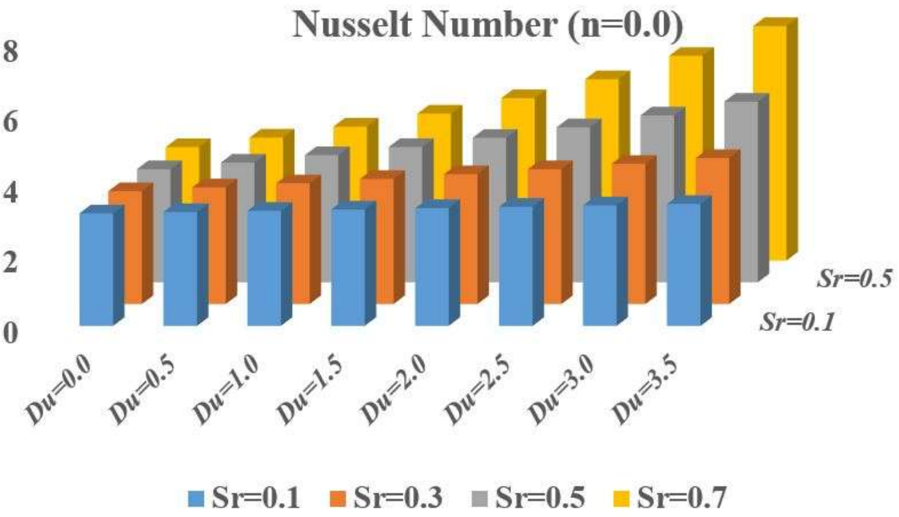

Figure 11: Variation of Nusselt number for different values of Dufour and Soret effects for $n = 0.0$.

Tables 2-3 show the skin friction, Nusselt number, and Sherwood number are influenced by various factors such as Dufour impact, Soret effect, Schmidt number, Prandtl number, curvature, micropolar factor, magnetic field, Sutterby fluid factor, and Casson fluid for both case $n = 0.0$ and $n = 0.5$. Heat transfer values become high and mass transfer values become low due to increment in the Dufour number while friction at surface found to be no changes. Heat transfer values become high and mass transfer values become low due to increment in the Soret number while friction at surface found to be no changes. The friction at surface become fixed due to changes values of Schmidt number. The heat and mass transfer rate become high due to increasing values of Schmidt number. The friction at surface become fixed due to changes values of Prandtl number. The heat transfer values become high and mass transfer values become high due to increasing values of Prandtl number. Heat transfer values and mass transfer values become low due to higher values of curvature factor. Magnitude of friction at surface become low due to higher values of curvature. Heat transfer values and mass transfer values become low due to higher values of micropolar factor. Magnitude of friction at surface become low due to higher values of micropolar factor. Heat transfer values and mass transfer values become low due to higher values of magnetic field. Magnitude of friction at surface become high due to higher values of magnetic field. Heat transfer values and mass transfer values become high due to higher values of Sutterby factor. Magnitude of friction at surface become low due to higher values of Sutterby factor. Depending on Sutterby parameters, the fluid can display shear-thinning or shear-thickening behavior in the fluids. Shear-thinning fluids become less viscous with higher shear rates, improving the heat and mass transfer rate by making it easier for the fluid to flow and transport heat and mass. On the other hand, shear-thickening fluids increase in viscosity with increasing shear rates, which can hinder heat and mass transfer. As the Sutterby factor increases, the fluid may show more pronounced shear-thinning behavior, meaning that the fluid's viscosity decreases as the shear rate increases. A lower viscosity in the fluid leads to less flow resistance, and as a result, a lower shear stress (or friction) occurs at the surface. Heat transfer values and mass transfer values become low due to higher values of Casson factor. Magnitude of friction at surface become low due to higher values of Casson factor. As the Casson factor increases, the fluid's velocity profile near the stretching surface becomes flatter.

This indicates slower fluid motion, reducing heat and mass convective transport, resulting in lower transfer rates. When the Casson factor is higher, it means that the fluid has a higher yield stress. This higher yield stress causes the fluid to behave like a solid even at low shear rates, making it more difficult for the fluid to flow near the stretching surface. Tables 4-5 display the comparative findings of the current analysis in relation to the literature. The presented results focus on the heat transfer aspect and compare different Prandtl number values while maintaining constant values for all other parameters. These findings are compared to the study conducted by Elbashbeshy [30] like as $\beta = 1000$, $\Gamma_0 = 0.0$, $\gamma = 0.0$, $Sr = 0.0$, $Du = 0.0$, $\Gamma = 1000$ which revealed in Table 4. Comparative heat transfer results are depicted for varying Prandtl numbers while maintaining constant values for all other parameters, in comparison with Okechi et al. [24] like as $\beta_0 = 10000000$, $\Gamma_0 = 0.0$, $\gamma = 0.0$, $Sr = 0.0$, $Du = 0.0$, $Pr = 0.0$ which revealed in Table 5.

Table 2: Numerical results of the impact of physical factors on the skin friction, Nusselt number, and Sherwood number for $n = 0.5$.

Du	Sr	Sc	Pr	Γ	Γ_0	M	γ	β_0	$C_f Re^{1/2}$	$NuRe^{-1/2}$	$ShuRe^{-1/2}$
0.0	0.4	0.2	1.5	1.0	0.4	0.4	0.3	0.5	-5.055789	2.191864	0.5167268
0.3	-	-	-	-	-	-	-	-	-5.055789	2.244215	0.5127853
0.6	-	-	-	-	-	-	-	-	-5.055789	2.298994	0.5086544
0.9	-	-	-	-	-	-	-	-	-5.055789	2.356380	0.5043199
0.3	0.0	-	-	-	-	-	-	-	-5.055789	2.182717	2.182717
-	0.4	-	-	-	-	-	-	-	-5.055789	2.244215	0.5127853
-	0.8	-	-	-	-	-	-	-	-5.055789	2.309097	0.3627339
-	1.2	-	-	-	-	-	-	-	-5.055789	2.377638	0.2021652
-	0.4	0.0	-	-	-	-	-	-	-5.055789	1.895924	0.3284587
-	-	0.2	-	-	-	-	-	-	-5.055789	2.244215	0.5127853
-	-	0.4	-	-	-	-	-	-	-5.055789	2.585752	0.6123586
-	-	0.6	-	-	-	-	-	-	-5.055789	2.934385	0.6437830
-	-	0.2	1.5	-	-	-	-	-	-5.055789	2.244215	0.5127853
-	-	-	2.0	-	-	-	-	-	-5.055789	2.630538	0.483639
-	-	-	3.0	-	-	-	-	-	-5.055789	3.275842	0.4343722
-	-	-	1.5	0.5	-	-	-	-	-7.854818	2.379075	0.6768338
-	-	-	-	1.0	-	-	-	-	-5.055789	2.244215	0.5127853
-	-	-	-	1.5	-	-	-	-	-3.871595	2.197173	0.4604141
-	-	-	-	2.0	-	-	-	-	-3.254115	2.171200	0.4346277
-	-	-	-	1.0	0.0	-	-	-	-5.489389	2.253153	0.5178094
-	-	-	-	-	0.4	-	-	-	-5.055789	2.244215	0.5127853
-	-	-	-	-	0.8	-	-	-	-4.308057	2.237238	0.5091624
-	-	-	-	-	1.2	-	-	-	-3.248081	2.231091	0.5060432
-	-	-	-	-	0.4	0.0	-	-	-4.44223	2.336665	0.585347
-	-	-	-	-	-	0.4	-	-	-5.055789	2.244215	0.5127853
-	-	-	-	-	-	0.8	-	-	-5.377799	2.191024	0.4860939
-	-	-	-	-	-	1.2	-	-	-5.623126	2.148553	0.4663283
-	-	-	-	-	-	0.4	0.0	-	-5.83474	2.216879	0.5042869
-	-	-	-	-	-	-	0.3	-	-5.055789	2.244215	0.5127853
-	-	-	-	-	-	-	0.6	-	-4.511408	2.265732	0.5262738
-	-	-	-	-	-	-	0.9	-	-4.098125	2.283130	0.5262738
-	-	-	-	-	-	-	0.3	0.5	-5.055789	2.244215	0.5127853
-	-	-	-	-	-	-	-	1.0	-3.617431	2.077665	0.4913074
-	-	-	-	-	-	-	-	1.5	-3.122097	2.188736	0.4855229

Du	Sr	Sc	Pr	Γ	Γ_0	M	γ	β_0	$C_f Re^{1/2}$	$NuRe^{-1/2}$	$ShuRe^{-1/2}$
-	-	-	-	-	-	-	-	2.0	-2.869778	2.177090	0.4806450

Table 3: Numerical results of the impact of physical factors on the skin friction, Nusselt number, and Sherwood number for $n = 0.0$.

Du	Sr	Sc	Pr	Γ	Γ_0	M	γ	β_0	$C_f Re^{1/2}$	$NuRe^{-1/2}$	$ShuRe^{-1/2}$
0.0	0.4	0.2	1.5	1.0	0.4	0.4	0.3	0.5	-4.958056	2.204198	0.5224746
0.3	-	-	-	-	-	-	-	-	-4.958056	2.256478	0.5185415
0.6	-	-	-	-	-	-	-	-	-4.958056	2.311183	0.5144192
0.9	-	-	-	-	-	-	-	-	-4.958056	2.368491	0.5100934
0.3	0.0	-	-	-	-	-	-	-	-4.958056	2.194911	0.6593843
-	0.4	-	-	-	-	-	-	-	-4.958056	2.256478	0.5185415
-	0.8	-	-	-	-	-	-	-	-4.958056	2.321429	0.3690208
-	1.2	-	-	-	-	-	-	-	-4.958056	2.390033	0.206996
-	0.4	0.0	-	-	-	-	-	-	-4.958056	1.907002	0.3284587
-	-	0.2	-	-	-	-	-	-	-4.958056	2.256478	0.5185415
-	-	0.4	-	-	-	-	-	-	-4.958056	2.598005	0.6213272
-	-	0.6	-	-	-	-	-	-	-4.958056	2.945949	0.6547849
-	-	0.2	1.5	-	-	-	-	-	-4.958056	2.256478	0.5185415
-	-	-	2.0	-	-	-	-	-	-4.958056	2.642283	0.4894581
-	-	-	3.0	-	-	-	-	-	-4.958056	3.286885	0.4402654
-	-	-	1.5	0.5	-	-	-	-	-7.802314	2.394297	0.6817800
-	-	-	-	1.0	-	-	-	-	-4.958056	2.256478	0.5185415
-	-	-	-	1.5	-	-	-	-	-3.763934	2.207758	0.4661453
-	-	-	-	2.0	-	-	-	-	-3.144411	2.180878	0.4402419
-	-	-	-	1.0	0.0	-	-	-	-5.489389	2.253153	0.5178094
-	-	-	-	-	0.4	-	-	-	-4.958056	2.256478	0.5185415
-	-	-	-	-	0.8	-	-	-	-4.118771	2.256658	0.5175819
-	-	-	-	-	1.2	-	-	-	-2.964114	2.256028	0.5163727
-	-	-	-	-	0.4	0.0	-	-	-4.32883	2.345862	0.5943681
-	-	-	-	-	-	0.4	-	-	-4.958056	2.256478	0.5185415
-	-	-	-	-	-	0.8	-	-	-5.280399	2.209143	0.493777
-	-	-	-	-	-	1.2	-	-	-5.526441	2.163655	0.4758721
-	-	-	-	-	-	0.4	0.0	-	-5.67609	2.232930	0.5113329
-	-	-	-	-	-	-	0.3	-	-4.958056	2.256478	0.5185415
-	-	-	-	-	-	-	0.6	-	-4.445951	2.275501	0.5248666
-	-	-	-	-	-	-	0.9	-	-4.05215	2.291314	0.5305075
-	-	-	-	-	-	-	0.3	0.5	-4.958056	2.256478	0.5185415
-	-	-	-	-	-	-	-	1.0	-3.527022	2.226899	0.5021185
-	-	-	-	-	-	-	-	1.5	-3.036428	2.212181	0.4948888
-	-	-	-	-	-	-	-	2.0	-2.787315	2.203329	0.4907954

Table 4: Different values of Pr were compared in terms of heat transfer with Elbashbeshy [30]

while keeping all other variables constant like as $\beta_0 = 1000$, $\Gamma_0 = 0.0$, $\gamma = 0.0$, $Du = 0.0$, $Sr = 0.0$, $\Gamma = 1000$.

Pr	Elbashbeshy [30]	Present Analysis
0.720	0.4347170	0.43036949
1.00	0.5496410	0.53691702
3.00	1.1220900	1.04264899
10.00	2.2574300	1.93437061

Table 5: Different values of Γ were compared in terms of heat transfer with Okechi et al. [24] while keeping all other variables like as $\beta_0 = 10000000$, $\Gamma_0 = 0.0$, $\gamma = 0.0$, $Sr = 0.0$, $Du = 0.0$.

Γ	Current Study	Okechi et al. [24]
5.00	1.4119108	1.4196000
10.00	1.3281841	1.3467000
20.00	1.29876087	1.3135000

5. Conclusions

We have analyzed the flow of Sutterby micropolar Casson fluid over an exponentially stretching curved sheet, focusing on dynamic analysis. The study analyzed the Soret and Dufour effects and considered the impact of a very low magnetic Reynolds number. The governing mathematical model have been solved through numerical scheme. The main key points of the analysis are presented below:

- Casson fluid revealed shear thinning behavior, which decreased viscosity with increasing shear rate. As the Casson fluid parameter increased and the impact on flow dynamics became more pronounced which led to a greater velocity decline.
- Sutterby fluid parameter increased, which led to an increase in the velocity of the fluid close to the stretching surface. These changes occurred because the fluid resistance to deformation decreased, allowing it to flow more freely. As a result, the velocity within the boundary layer can increase.
- Temperature are noted to be declining for higher values of Dufour effect. As a result of transfer, the high-concentration regions have had higher temperatures and lost heat energy. This loss of energy caused into decrease in temperature in these regions.
- Temperature are noted to be declining for higher values of Prandtl number. As the Prandtl number increased, the fluid conducted less heat relative to its motion. A higher Prandtl number also formed a thicker thermal boundary layer. As a result, the heat transfer rate decreased.
- Our results found to be good agreed with decay literature.

Nomenclature

(x, S) (m)	Curvilinear Coordinates	θ (1)	Temperature
V, W (m/s)	Velocity Components	g (1)	Micro-Rotation
a^* (m)	Length Of Stretching Sheet	N	Micro-Rotation Component
V_w (m/s)	Velocity At Wall	β_0 (1)	Casson Fluid Factor
σ_0 (J/K)	Boltzmann Contact	Pr (1)	Prandtl Factor
K_1 (m)	Curvature Of Curved Surface	γ (1)	Sutterby Fluid Factor
T_w (K)	Temperature At Wall	Γ (1)	Curvature Factor
T_∞ (K)	Ambient Temperature	M (1)	Magnetic Field Factor
ν_f (m^2/s)	Kinematic Viscosity	P (Pa)	Pressure
ρ_f (kg/m^3)	Fluid Density	Nu (1)	Nusselt Number
μ_f (m^2/s)	Dynamic Viscosity	τ_{xs} (Pa)	Wall Shear Stress
Γ_0 (1)	Micropolar Fluid Factor	q_w (W/m^2)	Heat Flux
k^* (Ns/m^2)	Vortex Viscosity	Re (1)	Local Reynolds Number
C_{p_f} (J/kgK)	Specific Heat Capacitance	θ (1)	Temperature
T (K)	Prescribed Temperature	ξ (1)	Similarity Variable

Declarations

Availability of data and materials: The data and material are available and can be shared upon request.

Conflict of interest: The authors declare that they have no known competing financial interests or personal relationships that could have appeared to influence the work reported in this paper.

Authors' contributions: Nadeem Abbas is helped in writing and reviewing, analysis data, data Collection, proofreading. Wasfi Shatanawi is helped in proofreading, editing, methodology, finalizing and also supervised. M.Y.B. Mufarrej is helped in software, methodology, writing, review and proofreading.

Acknowledgements

The authors would like to thank Prince Sultan University for their support through the TAS research lab.

References

[1] J. L. Sutterby. Laminar converging flow of dilute polymer solutions in conical sections: Part i. viscosity data, new viscosity model, tube flow solution. *AIChE Journal*, 12(1):63–68, 1966.

[2] F. Tetsu, M. Osamu, F. Motoo, T. Hiroshi, and M. Kentaro. Natural convective heat transfer from a vertical isothermal surface to a non-newtonian sutterby fluid. *International Journal of Heat and Mass Transfer*, 16(12):2177–2187, 1973.

[3] T. Hayat, H. Zahir, M. Mustafa, and A. Alsaedi. Peristaltic flow of sutterby fluid in a vertical channel with radiative heat transfer and compliant walls: a numerical study. *Results in Physics*, 6:805–810, 2016.

[4] M. Sohail and R. Naz. Modified heat and mass transmission models in the magnetohydrodynamic flow of sutterby nanofluid in stretching cylinder. *Physica A: Statistical Mechanics and its Applications*, 549:124088, 2020.

[5] B. Ishtiaq, S. Nadeem, and J. Alzabut. Effects of variable magnetic field and partial slips on the dynamics of sutterby nanofluid due to biaxially exponential and nonlinear stretchable sheets. *Heliyon*, 9(7), 2023.

[6] N. Abbas, W. Shatanawi, F. Hasan, and Z. Mustafa. Thermal analysis of radiative sutterby nanofluid flow over stretching curved surface. *Heliyon*, 10(13), 2024.

[7] K. Srihari, B. S. Goud, and T. L. Babu. Significance of chemical reaction and velocity slip on magnetized sutterby nanofluid over stretchable sheet. *Results in Engineering*, page 105564, 2025.

[8] R. G. Mortimer and H. Eyring. Elementary transition state theory of the soret and dufour effects. *Proceedings of the National Academy of Sciences*, 77(4):1728–1731, 1980.

[9] A. Postelnicu. Influence of a magnetic field on heat and mass transfer by natural convection from vertical surfaces in porous media considering soret and dufour effects. *International Journal of Heat and Mass Transfer*, 47(6–7):1467–1472, 2004.

[10] M. K. Partha, P. V. S. N. Murthy, and G. P. Raja Sekhar. Soret and dufour effects in a non-darcy porous medium. 2006.

[11] H. Sardar, L. Ahmad, M. Khan, and A. S. Alshomrani. Investigation of mixed convection flow of carreau nanofluid over a wedge in the presence of soret and dufour effects. *International Journal of Heat and Mass Transfer*, 137:809–822, 2019.

[12] N. Jiang, E. Studer, and B. Podvin. Physical modeling of simultaneous heat and mass transfer: species interdiffusion, soret effect and dufour effect. *International Journal of Heat and Mass Transfer*, 156:119758, 2020.

[13] M. S. Abbas, A. Shaheen, N. Abbas, and W. Shatanawi. Mathematical model of second-grade casson fluid flow with soret and dufour impact over riga sheet. *Modern Physics Letters B*, 38(25):2450230, 2024.

[14] M. Ali, N. Abbas, and W. Shatanawi. Soret and dufour effects on sutterby nanofluid flow over a riga stretching surface with variable thermal conductivity. *Modern Physics Letters B*, 39(14):2450455, 2025.

[15] K. Vajravelu, K. V. Prasad, H. Vaidya, N. Z. Basha, and C. O. Ng. Mixed convective flow of a casson fluid over a vertical surface. *Applied Mathematics and Computation*, 184:864–873, 2007.

[16] S. Mukhopadhyay, P. R. De, K. Bhattacharyya, and G. C. Layek. Casson fluid flow over an unsteady stretching surface. *Ain Shams Engineering Journal*, 4(4):933–938, 2013.

[17] I. S. Oyelakin, S. Mondal, and P. Sibanda. Unsteady casson nanofluid flow over a stretching sheet. *Alexandria Engineering Journal*, 55(2):1025–1035, 2016.

[18] P. Kumar, B. Nagaraja, F. Almeida, A. R. AjayKumar, Q. Al-Mdallal, and F. Jarad. Magnetic dipole effects on unsteady flow of casson-williamson nanofluid. *Scientific Reports*, 13:12770, 2023.

[19] A. Wahab, M. I. Asjad, K. Anjum, and S. Khan. Computational modeling of casson blood flow in symmetrically stenosed carotid arteries. *Punjab University Journal of Mathematics*,

57(1):43–63, 2025.

[20] H. U. Rasheed, S. Islam, Zeeshan, T. Abbas, and J. Khan. Analytical treatment of mhd flow and chemically reactive casson fluid. *Waves in Random and Complex Media*, 35(2):2332–2348, 2025.

[21] M. Sajid and T. Hayat. Influence of thermal radiation on boundary layer flow due to exponentially stretching sheet. *International Communications in Heat and Mass Transfer*, 35(3):347–356, 2008.

[22] B. Sahoo and S. Poncet. Flow and heat transfer of a third grade fluid past an exponentially stretching sheet. *International Journal of Heat and Mass Transfer*, 54(23–24):5010–5019, 2011.

[23] M. Mustafa, M. A. Farooq, T. Hayat, and A. Alsaedi. Numerical and series solutions for stagnation-point flow of nanofluid. *PLoS ONE*, 8(5):e61859, 2013.

[24] N. F. Okechi, M. Jalil, and S. Asghar. Flow of viscous fluid along exponentially stretching curved surface. *Results in Physics*, 7:2851–2854, 2017.

[25] S. Islam, M. Jawad, K. C. Gokul, M. Zubair, H. Alrabaiah, Z. Shah, and A. Saeed. Entropy optimization in mhd nanofluid flow over curved exponentially stretching surface. *Journal of Physics Communications*, 4(7):075021, 2020.

[26] A. R. Ajaykumar, P. Kumar, F. Almeida, B. Nagaraja, and Q. Al-Mdallal. Sensitivity analysis and entropy optimization in nanofluid flow. *International Journal of Thermofluids*, page 100668, 2024.

[27] S. Nadeem, Y. S. Hamed, M. B. Riaz, I. Ullah, and J. Alzabut. Finite element method for natural convection flow of casson hybrid nanofluid. *AIP Advances*, 14(8), 2024.

[28] N. Abbas, W. Shatanawi, and T. A. Shatnawi. Thermodynamic properties of casson-sutterby-micropolar fluid flow. *Case Studies in Thermal Engineering*, page 104123, 2024.

[29] Fatima. N, Majeed. A, Ijaz. N, Ghodhbani. R, and Saleem. N. Thermal performance of cattaneo-christov heat flux model on 3d micropolar fluid with motile microbes across a permeable surface. *BioNanoScience*, 14:2419–2434, 2024.

[30] E. M. A. Elbashbeshy. Heat transfer over exponentially stretching surface with suction. *Archives of Mechanics*, 53(6):643–651, 2001.